remote sensing

MDPI

Article

Glacier Mass Balance and Its Impact on Land Water Storage in the Southeastern Tibetan Plateau Revealed by ICESat-2 and GRACE-FO

Jinwei Tong [1], Zhen Shi [1,*], Jiashuang Jiao [2,3], Bing Yang [1] and Zhen Tian [1]

[1] College of Geological Engineering and Geomatics, Chang'an University, Xi'an 710054, China; jinwei.tong@chd.edu.cn (J.T.); bing.yang@chd.edu.cn (B.Y.); zhen.tian1990@hotmail.com (Z.T.)
[2] Wuhan Gravitation and Solid Earth Tides National Observation and Research Station, Wuhan 430071, China; jiashuang.jiao@whu.edu.cn
[3] School of Geodesy and Geomatics, Wuhan University, Wuhan 430079, China
* Correspondence: shizhen@chd.edu.cn; Tel.: +86-029-82339032

Abstract: The southeastern Tibetan Plateau (SETP), which hosts the most extensive marine glaciers on the Tibetan Plateau (TP), exhibits enhanced sensitivity to climatic fluctuations. Under global warming, persistent glacier mass depletion within the SETP poses a risk to water resource security and sustainability in adjacent nations and regions. This study deployed a high-precision ICESat-2 satellite altimetry technique to evaluate SETP glacier thickness changes from 2018 to 2022. Our results show that the average change rate in glacier thickness in the SETP is -0.91 ± 0.18 m/yr, and the corresponding glacier mass change is -7.61 ± 1.52 Gt/yr. In the SETP, the glacier mass loss obtained via ICESat-2 data is larger than the mass change in total land water storage observed by the Gravity Recovery and Climate Experiment follow-on satellite (GRACE-FO), -5.13 ± 2.55 Gt/yr, which underscores the changes occurring in other land water components, including snow (-0.44 ± 0.09 Gt/yr), lakes (-0.06 ± 0.02 Gt/yr), soil moisture (1.88 ± 1.83 Gt/yr), and groundwater (1.45 ± 0.70 Gt/yr), with a closure error of -0.35 Gt/yr. This demonstrates that this dramatic glacier mass loss is the main reason for the decrease in total land water storage in the SETP. Generally, there are decreasing trends in solid water storage (glacier and snow) against stable or increasing trends in liquid water storage (lakes, soil moisture, and groundwater) in the SETP. This persistent decrease in solid water is linked to the enhanced melting induced by rising temperatures. Given the decreasing trend in summer precipitation, the surge in liquid water in the SETP should be principally ascribed to the increased melting of solid water.

Keywords: satellite altimetry; ICESat-2; GRACE-FO; glacier mass balance; southeastern Tibetan Plateau

Citation: Tong, J.; Shi, Z.; Jiao, J.; Yang, B.; Tian, Z. Glacier Mass Balance and Its Impact on Land Water Storage in the Southeastern Tibetan Plateau Revealed by ICESat-2 and GRACE-FO. *Remote Sens.* **2024**, *16*, 1048. https://doi.org/10.3390/rs16061048

Academic Editors: Mohammad Bagherbandi, Robert Tenzer and Hok Sum Fok

Received: 2 February 2024
Revised: 8 March 2024
Accepted: 13 March 2024
Published: 15 March 2024

1. Introduction

The Tibetan Plateau has the most concentrated area of land glaciers, except for Antarctica and Greenland, and is known as "the third pole of the world" [1–3]. Abundant glacier resources provide important freshwater resources for high-altitude areas and are also a major component of the cryosphere [4–6]. Owing to their high sensitivity to climatic variations, glaciers serve as key indicators of climate change [7]. The ongoing global climate dynamics have precipitated pronounced morphological transformations in these glaciers, notably marked by their contraction and thinning [6,8–10]. The intensified melting of glaciers increases intra-annual and inter-annual variations in water resources, which may cause long-term water supply shortages in the future [11–13]. Furthermore, these changes pose a heightened risk for natural calamities, including glacial lake outbursts, ice collapses, and debris flows, which gravely endanger the livelihoods of downstream communities, as well as their socio-economic fabric [14,15]. Hence, intensifying glacier monitoring is imperative for effective water resource management and natural disaster mitigation.

The southeastern Tibetan Plateau (SETP) is a region where marine glaciers are concentrated. The abundant glaciers in the SETP are important water supply sources, providing important freshwater resources for millions of people [16,17]. Compared with continental glaciers, marine glaciers are more sensitive to climate change [3,18,19]. The escalating global warming phenomenon has led to a pronounced decline in glacier mass in the SETP, approximately tripling the mean loss rate observed across the Tibetan Plateau [15,20,21]. The dramatic melting of marine glaciers and their active surface movement have changed the occurrence frequency and hazard range of natural disasters such as ice collapses, glacial lake outbursts, debris flows, and landslides in the SETP, which have affected the water security, infrastructure security, and ecological security of rivers along and downstream from the SETP [22]. The traditional methods for monitoring glacier mass change principally include the following two types [10]: (1) the glaciological estimation method and (2) the glacier model approach. Glaciological estimation, which is rooted in field observations, faces significant challenges due to geographical conditions that can limit its application for estimating small-scale and long-term glacier mass balance [1,8]. The glacier model approach predicts changes in glaciers by integrating detailed climate data with numerous observations, but it is applicable mainly to glaciers with extensive field observations [23]. Although these methods enable more direct and precise monitoring of glacier mass balance, their utility is considerably restricted in regions with complex terrain such as the SETP, which allows for a very limited number of in situ observations [24]. Contemporary satellite remote sensing technology offers a more viable approach for small-scale glacier monitoring because it overcomes the limitations presented by geographical conditions, particularly for glacier regions with limited possibilities for in situ observation [25]. Currently, satellite-based glacier monitoring in the SETP can be categorized into three principal methods. The first method utilizes multiple digital elevation model (DEM) datasets, acquired at various time points, to deduce glacier elevation alterations by differencing DEM datasets. Considering other methods, this method is based on stereo image data and can rapidly observe glaciers over a large range; it is a common method for monitoring glacier elevation changes. Nonetheless, the temporal resolution constraints inherent in DEM data impose limitations on their efficacy for prolonged time series analysis [26–28]. Ren et al. [29] employed three-dimensional imagery produced by the ZY-3 satellite to investigate mass changes in the Nyainqentanglha Mountains Glacier. The findings indicated a mean elevation alteration rate of -0.66 ± 0.24 m/yr. The second method for satellite-based glacier monitoring involves measuring the earth's time-varying gravity field using Gravity Recovery and Climate Experiment (GRACE) satellite gravity facilitating glacier mass change inversion. However, GRACE observations of SETP glaciers are subject to interference from regional hydrological mass changes, such as fluctuating lake levels and soil moisture content [17,30,31]. To address this, Yi et al. [17] employed empirical orthogonal decomposition to separate hydrological signals from glacier and snow data in the SETP, revealing a long-term trend of -6.5 ± 0.8 Gt/yr in ice and snow mass. Similarly, Jiao [32] and He [33] utilized GRACE data alongside hydrological models to investigate seasonal glacier variations in the Tibetan Plateau, determining a glacier mass loss rate of -4.20 ± 0.57 Gt/yr or -6.33 ± 0.54 Gt/yr for the SETP. The third method involves measuring glacier surface elevation through satellite altimetry, as demonstrated by the ICESat (Ice, Cloud, and Land Elevation Satellite). This approach, when combined with other elevation datasets, allows for detailed analysis of glacial elevation variations. For instance, Kaab et al. [34] employed ICESat and SRTMDEM data to study mountain glacier elevation changes, revealing a mass loss of -4.69 ± 2.03 Gt/yr in the SETP glaciers from 2003 to 2009 [5,35,36]. Nonetheless, the limited spatial sampling of the ICESat-1 could lead to biased outcomes [37]. Addressing this limitation, the ICESat-2 (2018 to present), equipped with an advanced laser system, yields a significantly higher number of annual footprint points, approximately 150 times more than the ICESat-1 [25]. Consequently, the ICESat-2 enhances the accuracy in quantifying glacial mass changes [38].

Previous research has established the viability of using the above research methods for monitoring glacier mass variations. Although ICESat-1 data have confirmed that glaciers in this region continued to melt from 2003 to 2009, whether this speed of glacier loss has increased recently has not been well quantified. The ICESat-2, which started in 2018, can help to constrain current glacier change. In order to further study glacier mass changes in the SETP, some researchers have integrated data from both the ICESat and GRACE. Song et al. [5] used ICESat and GRACE data to construct the time series of glacier mass change in this region from 2003 to 2009. Wang et al. [25] combined ICESat, ICESat-2, GRACE, and GRACE-FO data to observe the glacier ablation in Nyainqentanglha Mountain, and the results showed that the two methods have their own advantages in acquiring glacier signals. However, most studies applying the above methods mainly focus on the quantification of glacier mass change, and there is still a lack of deep understanding of the relationship between glacier mass loss and changes in land water storage in the SETP.

In this study, we attempted to fill this research gap using a combination of ICESat-2 and GRACE-FO data. First, ICESat-2 data were used to construct and analyze the time series of glacier elevation change and glacier mass change in the SETP from 2018 to 2022. Subsequently, GRACE-FO data were used to evaluate the total land water mass change within the SETP, and the impact of glacier change on land water storage was analyzed, considering multiple hydrological components including soil moisture, snow, lakes, and groundwater.

2. Study Area

The glaciated region within the southeastern Tibetan Plateau (SETP) (Figure 1) encompasses the Nyainqentanglha Mountains and the Eastern Himalayas. These areas have developed intricate topography and geomorphological features due to the ongoing tectonic compression between the Eurasian and Indian plates. With an average elevation exceeding 4000 m and an annual mean temperature of approximately 0 °C, the SETP exhibits a unique climatic profile characterized by high altitudes and low temperatures, fostering the accumulation of a substantial number of glaciers. Geographically, this region extends from 89.11° to 98.27°E and 27.54° to 31.44°N. Based on the glacier type classification from the Chinese Glacier Catalog [24,39], the SETP predominantly features marine glaciers, totaling 9686 glaciers covering an approximate area of 9298 km^2 (RGI 6.0) [40]. Among them, there are 120 glaciers with an area of more than 10 km^2, for a total area of 3012 km^2. In the context of global warming, glaciers in the SETP have experienced long-term serious melting and some large glaciers have become several small glaciers separated by ridgelines, resulting in the emergence of many small glaciers in the SETP [41]. The SETP is the intersection of multiple monsoon climates, which is mainly dominated by two climatic systems as follows: the westerly circulation and the Indian Ocean monsoon. During the dry period (November to March), the westerly circulation carries reduced moisture content, resulting in decreased precipitation. Conversely, from April to October each year, the region predominantly experiences the Indian Ocean monsoon climate, which is characterized by abundant precipitation that serves as the primary source of precipitation in the region, accounting for 60% to 90% of the annual total [5,42]. Simultaneously, the topographical features of valleys in the SETP create conduits for water vapor, enhancing precipitation and rendering this area one of the wettest regions within the Tibetan Plateau. In conclusion, the abundant precipitation in the SETP leads to the characteristics of high accumulation, high ablation, and strong activity for marine glaciers in this region. With the intensification and thinning of the melting of marine glaciers, the variability in subglacial water pressure and the coefficient of water pressure increase, which in turn leads to the strengthening of the sliding process at the bottom of the glacier, and the transport speed of the ice body to the lower elevations glacier area is relatively accelerated, which make the end of the glacier tongue extend to lower elevations [3]. Due to the high temperatures in lower elevations, the glacier tongue has experienced serious melting, exacerbating the glacier mass loss.

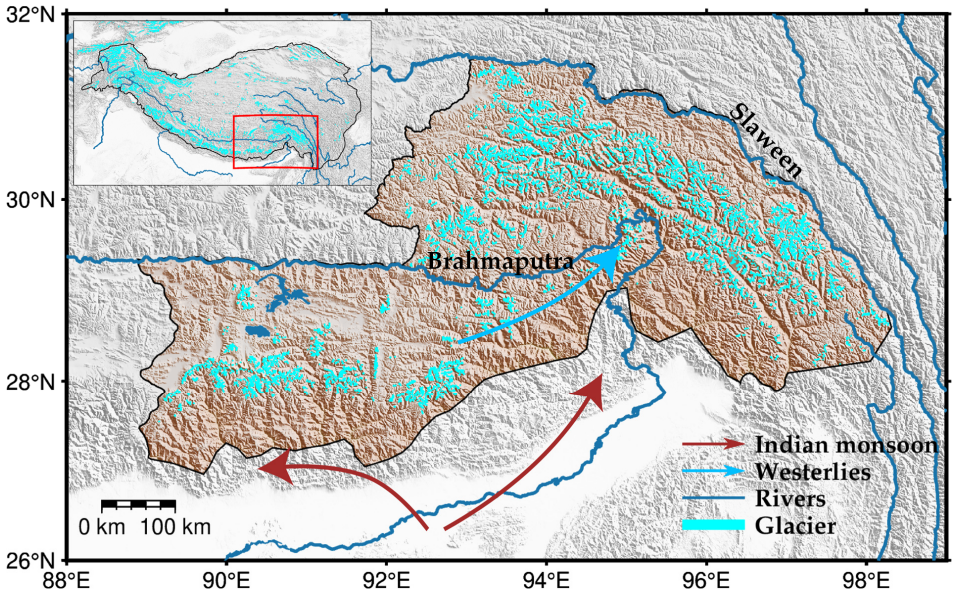

Figure 1. Geographical locations and distribution of glaciers in the southeastern Tibetan Plateau.

3. Data and Methods

In this study, we integrated multiple satellite datasets and hydrological models to analyze the glacier surface elevation changes and their impact on regional mass balance in the southeastern Tibetan Plateau (SETP). We utilized advanced ICESat-2 satellite altimetry to measure glacier surface elevation changes. Complementing this, Gravity Recovery and Climate Experiment follow-on (GRACE-FO) data were used to constrain the water mass change. Furthermore, we incorporate data from various hydrological models to infer mass changes in multiple land water components. The data processing flow is shown in Figure 2.

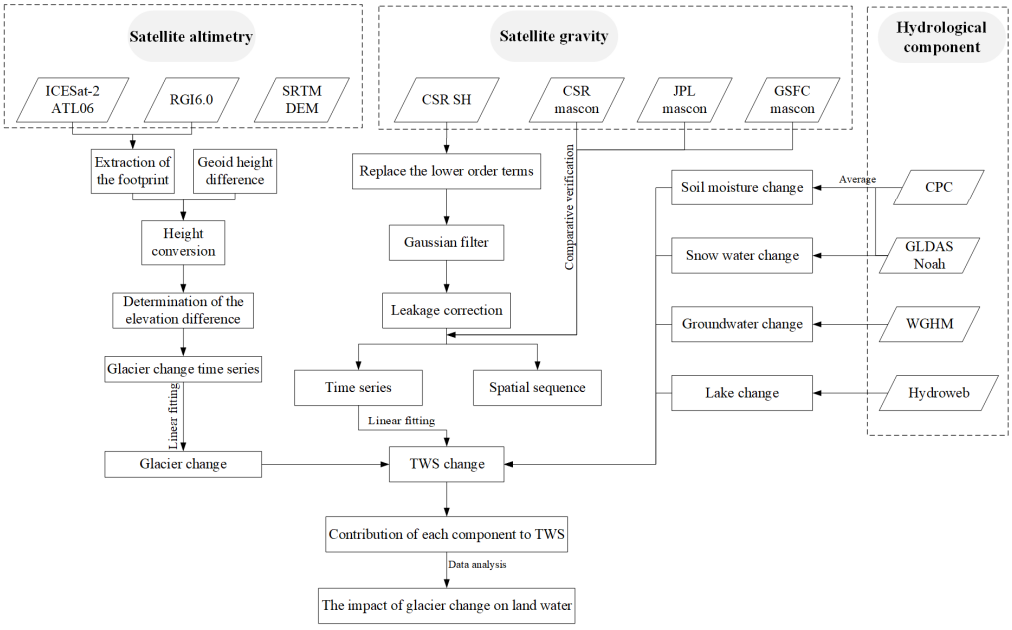

Figure 2. Flowchart of method.

3.1. ICESat-2 Data and Processing

In this research, we utilized ICESat-2 altimetry results to quantify changes in glacier elevation in the SETP [41]. The ICESat-2, the successor to the ICESat, was launched by NASA in September 2018. It is equipped with the Advanced Topographic Laser Altimeter System (ATLAS), which offers the highest altitude accuracy currently available in

space-borne LiDAR systems. Compared with the ICESat-1, the ICESat-2 shows significant improvements in data coverage density, data accuracy, and spatial resolution. In this study, ICESAT-2 L3A land ice elevation data (ATL06) were used to analyze SETP glacier thickness changes, which are available from the National Snow and Ice Data Center website (https://nsidc.org/data/ICESat-2, accessed on 19 April 2023).

The ATL06 data applied in this study provide surface elevation, longitude, latitude, and quality data for assessing height. Due to the ICESat sampling rate, track gap, and rugged terrain in the Tibetan Plateau, a reference DEM was used to correct for topographic differences in the ICESat sampling footprint [34]. The Shuttle Radar Topography Mission (SRTM) global 1-arc-second DEM, offering a spatial resolution of 30 m, served as our reference. These data, accessible via the USGS Earth Explorer website, underpinned our analysis (https://earthexplorer.usgs.gov/, accessed on 8 May 2023).

Data processing included the following six steps (Figure 3):

(1) Extract glacier footprint. We determined the footprint of the ICESat-2 within the glacier using RGI6.0 glacier boundary data.
(2) Height conversion. We converted the ICESat-2 footprint height based on the WGS-84 ellipsoid to the orthometric height based on EGM96 to be consistent with the coordinate system of the DEM ($H_{egm96} = H_{wgs84} - N_{geoid\ height}$).
(3) Determination of elevation difference. The SRTM elevation and slope of each ICESat footprint were extracted through the bilinear interpolation of DEM grid cells, and the elevation difference between ICESat-2 and SRTM data was obtained ($dh = H_{ICESat\text{-}2} - H_{SRTM} + H_p$). Because the DEM data of the SRTM have a penetration depth for the glacier, the penetration depth of $H_p = 1.5$ m was added back into this study [43].
(4) Outlier removal. To eliminate the abnormal points affected by cloud, fog, and terrain, we selected a threshold of 300 to remove the abnormal elevation difference, removed the measured points with a terrain slope greater than 30°, and retained the footprint points with mark 0 according to the official quality mark.
(5) Division of the elevation bins. We divided the glacier into multiple elevation bins with the same width and no overlap between each bin. The median elevation difference (dh) of all footprint points within each bin determined the elevation difference (Dh) for that bin.
(6) Estimate the average glacier surface elevation anomaly (DH). We used the ratio of the glacier area to the total glacier area of each elevation chamber as the weight ($P_i = S_i/S$, $P_1 + P_2 + P_3 + \ldots + P_n = 1$). Then, the weighted elevation differences across all bins were aggregated to yield the final elevation difference ($DH = P_1 \times Dh_1 + P_2 \times Dh_2 + P_3 \times Dh_3 + \ldots + P_n \times Dh_n$).

In our approach, the glacier was divided into distinct, non-overlapping elevation bins of 100 m each [41]. The DH change represents a time series of glacier thickness changes. A density of 900 ± 17 kg/m^3 [27,35] was used to convert glacier thickness changes into mass changes.

3.2. GRACE-FO Data

Launched on 22 May 2018, the GRACE-FO serves as the successor to the GRACE mission, a collaborative effort between NASA and the German Research Centre for Geosciences (GFZ). We adopted the monthly mascon solutions published by the following three institutions: The Center for Space Research (CSR) at the University of Texas [grid resolution $0.25° \times 0.25°$, approximately 27.75 km] (CSR-M), the Jet Propulsion Laboratory (JPL) [grid resolution $0.5° \times 0.5°$, approximately 55 km] (JPL-M), and the Goddard Space Flight Center (GSFC) [grid resolution $0.5° \times 0.5°$] (CSFC-M), to retrieve terrestrial water storage (TWS) anomalies in the SETP for the period from October 2018 to October 2022. These mascon solutions, compared with traditional spherical harmonic coefficients, enhance signal resolution and also significantly mitigate signal leakage errors [44], which have been widely used in hydrology fields. Nonetheless, the imperfect leakage correction of mascon solutions may still lead to an underestimation of the regional mass change trends [45]. For

comparison, we also estimated the TWS mass anomalies using the GRACE-FO spherical harmonic coefficient solutions (up to 60 degrees/order) released by CSR from October 2018 to October 2022. We first corrected the degree-1 (Technical Note TN-13), C20, and C30 coefficients (Technical Note TN-14) of the original GRACE-FO spherical harmonic coefficients. Then, a 300 km Gaussian filter was adopted to suppress the stripe noise. After that, we performed the leakage correction considering both the leakage-in and the leakage-out effects. For leakage-in correction, we first masked out the original signal within SETP and then smoothed the masked signal to estimate the leakage-in signal and deducted it from the original signal. For leakage-out correction, we corrected it by using the constrained forward modeling method [46] based on the signal after leakage-in correction [47].

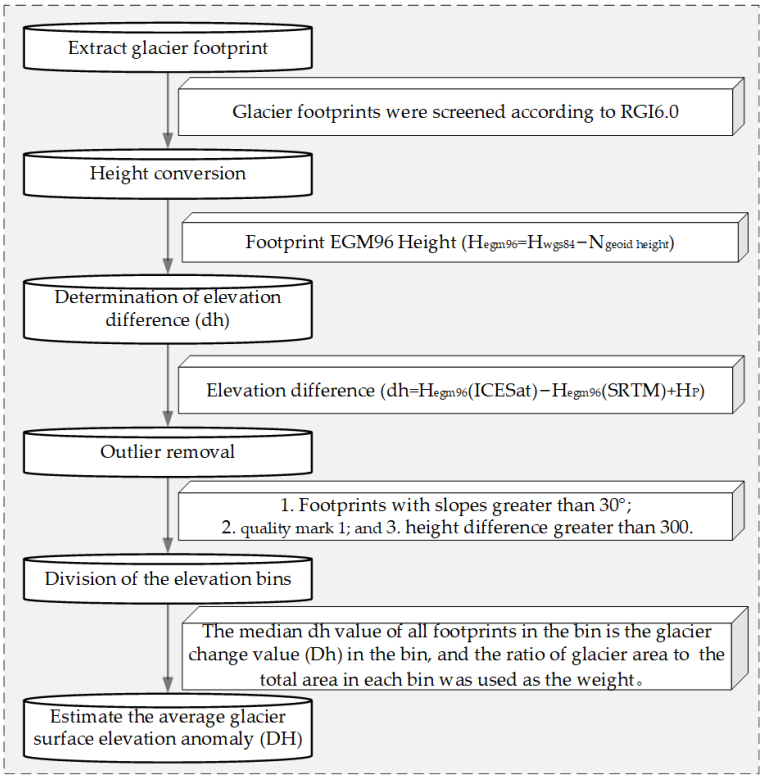

Figure 3. Flow diagram describing the processing steps for the ICESat-2 data to obtain valid footprints and calculate the glacier elevation difference.

3.3. Hydrological Model

The Global Land Data Assimilation System (GLDAS) is an advanced surface modeling system developed by the NASA Goddard Space Flight Center and the National Center for Environmental Prediction, which can be used to estimate surface states (soil moisture and temperature) and fluxes (evaporation). This study used GLDAS/Noah monthly output estimates of 4-layer soil moisture and snow water equivalent, with a grid resolution of 0.25° × 0.25°. Previous research by Bi et al. [48] indicated that the GLDAS model tended to systematically underestimate certain regions of the Tibetan Plateau compared with in situ observation data. To address this limitation, our study incorporated an additional hydrological model, the Climate Prediction Center (CPC) model, in conjunction with GLDAS for more accurate soil moisture data estimation. The CPC hydrological model was generated by the Climate Prediction Center according to the algorithm by Huang et al. [49]. Precipitation and temperature were used as meteorological inputs from CPC land precipitation reconstruction [50] and CPC global surface temperature analysis [51], respectively. The model uses more observation data, thus greatly improving the practicability. The CPC soil moisture data span the period from 1948 to the present, with a grid resolution of 0.5° × 0.5°.

The WaterGAP Global Hydrology Model (WGHM) stands as a vital tool in hydrological research, offering groundwater data spanning from 1981 to 2019 [52,53]. In this study, we used the WGHM to estimate the mass change rate of groundwater. Due to the lack of model data after 2019, only the monthly average data from 2018 to 2019 were used. To ensure stability, we conducted an examination of groundwater changes in the SETP from 2017 to 2019. This examination revealed a stable linear trend in groundwater changes.

3.4. Precipitation and Temperature Data

In this study, the Global Precipitation Climate Program (GPCP) [54] was used to simulate precipitation in the study area. The GPCP model offers gridded data at a grid resolution of 2.5° × 2.5° (http://www.esrl.noaa.gov/, accessed on 19 July 2023); we interpolated these data to become a grid resolution of 0.5° × 0.5°. Additionally, we utilized the ERA5-Land reanalysis dataset, disseminated by the European Centre for Medium-Range Weather Forecasts (ECMWF). This dataset represents a synthesis of simulated and observed data and provides multiple land variables on a 0.1° × 0.1° latitude/longitude grid. For consistency with the GPCP data, we also interpolated the ERA5-Land dataset to become a grid resolution of 0.5° × 0.5°. Our focus was on the following two specific variables from the ERA5-Land dataset: total precipitation and 2 m temperature (i.e., air temperature measured 2 m above the ground surface). These variables were selected due to their relevance to glacier thickness variations in the study region, and the data can be obtained from (https://cds.climate.copernicus.eu/#!/home, accessed on 19 July 2023).

3.5. Lake Data

In this study, we focused on YamdrokTso Lake within our research region in order to empirically assess the impact of glacial melt on lake dynamics [55]. As a result of missing part of the lake water level record data, the mean value of the data in the adjacent months was selected as the supplement. The lake data can be downloaded from (https://hydroweb.theia-land.fr/?lang=en&, accessed on 23 June 2023).

4. Results and Analysis

4.1. Glacier Thickness and Glacier Mass Change from ICESat-2 Measurements

Many studies have shown that the glacier mass change in the Tibetan Plateau has been seriously unbalanced since 2000, showing a long-term decreasing trend, which is roughly -17.53 ± 11.36 Gt/yr, with the most serious mass loss in the SETP [35]. Based on the ICESat-2 data, we obtained the time series of glacier surface elevation change in the SETP from October 2018 to October 2022, as shown in Figure 4a. The moving average method was used to improve the signal-to-noise ratio [56]. It can be seen that the change rate of glacier surface elevation in the SETP in the past four years is -0.91 ± 0.18 m/yr, and the corresponding mass change rate is -7.61 ± 1.52 Gt/yr. Figure 4a distinctly illustrates the variations in glacier thickness across the SETP, identifying a pattern of accumulation from winter to spring, peaking in spring, and a melting phase extending from summer to autumn, with the most significant losses occurring in the summer. Figure 4b,c provide further insights, depicting the rate of change in glacier surface elevation across various altitudes and the monthly count of valid footprint points from ICESat-2 data, respectively. The analysis of these footprint point distributions across different altitudes reveals a variable rate of glacier thickness reduction, with a notable correlation between the rate of change in glacier thickness and altitude. Specifically, the change rate of the thickness of glaciers below 4000 m increased gradually with increasing altitude, while the thickness of glaciers above 4000 m decreased gradually with increasing altitude, approaching a near-zero change in glacier elevation at altitudes ranging from 6000 to 6100 m above elevation, which means that the glacier melting and accumulation tend to balance at this elevation. In summary, the glacier surface elevation in the SETP showed a significant downward trend and great inter-annual variation during the study period.

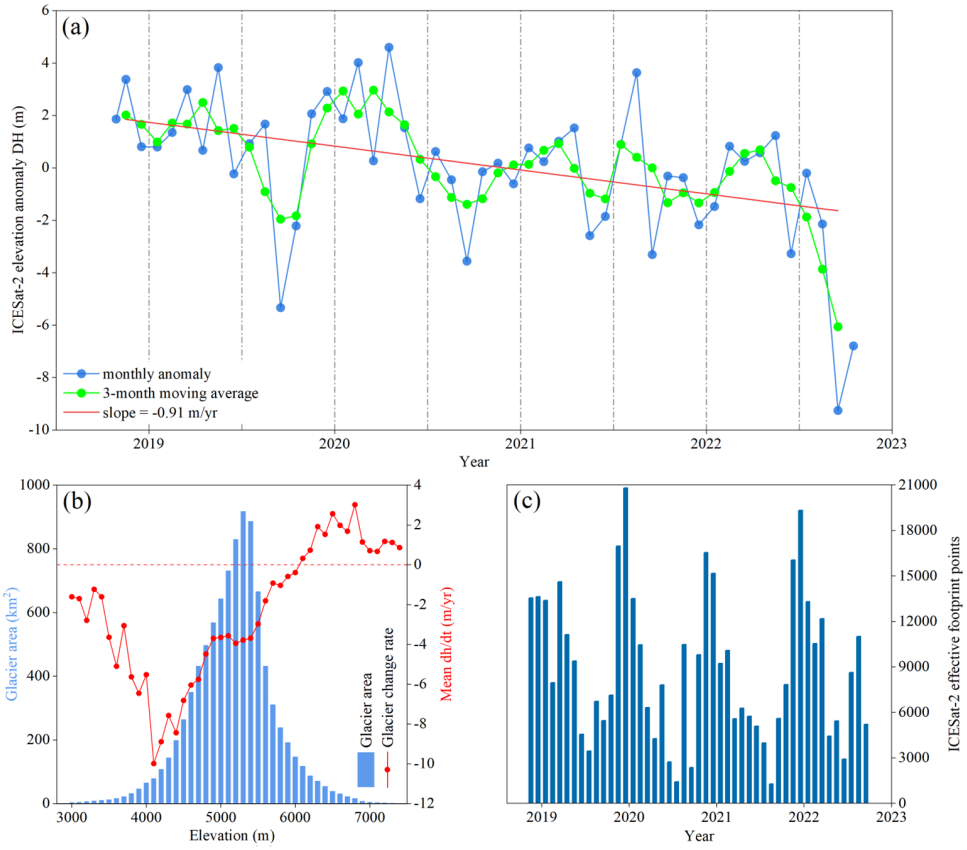

Figure 4. Glacier changes in the southeastern Tibetan Plateau (SETP) from October 2018 to October 2022. (**a**) Time series of SETP glacier surface elevation changes obtained by ICESat-2. (**b**) Elevation distribution of glacier surface elevation change rate. (**c**) Monthly valid footprint points.

In order to obtain the spatial distribution map of glacier changes in the SETP, we calculated the glacier thickness and glacier mass changes in a 0.25° × 0.25° grid (Figure 5). The results show that the glaciers in the SETP experienced significant mass loss from 2018 to 2022, and the distribution of glacier elevation change rate and mass change rate were significantly different. As illustrated in Figure 5a, the change rate in glacier elevation across the SETP exhibits a discernible gradient, gradually attenuating as one traverses the east to the west of the SETP. Combined with the distribution of the change rate at different altitudes, it was found that the main reason for this phenomenon is that glaciers in the west are distributed in regions with higher altitudes [3]. Furthermore, we observed that the elevation changes in the SETP glacier are closely related to its area size. The results indicate that the rate of elevation change in smaller glaciers scattered around the edges is more rapid in comparison with the loss experienced by larger, contiguous glaciers. The glacier mass change map in Figure 5b shows that the large-coverage glaciers in the SETP lose mass faster than the scattered small-coverage glaciers. This result indicates that although the faster thinning rate of small glaciers leads to rapid mass loss, their spatial coverage remains limited within the total glacier area. Consequently, large-coverage glaciers still play a dominant role in the glacier mass loss of the SETP.

4.2. Mass Loss in Southeast Tibet Observed by GRACE

In this study, we conducted a comparative analysis of equivalent water height (EWH) trend estimates derived from different GRACE-FO datasets (CSR, JPL, and GSFC). Our findings reveal that all four solutions effectively capture the spatio-temporal variations in terrestrial water storage (TWS) in the SETP for the period 2018–2022; moreover, the spatio-temporal variation trends as a whole showed strong consistency (Figure 6a–d). The maximum variation in TWS in the SETP during the four years was ±8 cm, indicating

that the spatial distribution was obviously heterogeneous. The TWS anomaly in the entire SETP was dominated by negative changes, showing a sharp decline in the east and a slow decline in the west. This shows good spatial consistency with the glacier mass change, as the glaciers are distributed more in the east and less in the west. In addition, the EWH results of the three mascons and spherical harmonic coefficients also show slight differences in local areas that are mainly reflected in the signal amplitude. It can be clearly seen that the TWS in the east part of the SETP is decreasing. The maximum decrease rate of the TWS in the east observed via CSR-M is -7.82 cm/yr, while the result obtained via JPL-M is about -4.96 cm/yr, and the result obtained via GSFC-M is only -3.0 cm/yr. Compared with the mascon products, the estimated decrease rate from the spherical harmonic coefficients after signal recovery reaches -7.96 cm/yr. Such a significant difference may be due to imperfect leakage correction in the mascon solutions; thus, this research used the calculation results from spherical harmonic coefficients to estimate the mass change in TWS (Figure 6d). Ultimately, the change rate in TWS in the SETP is estimated to be approximately -2.13 ± 1.05 cm/yr, indicating a total decrease trend in EWH. When factoring the area and the density of water, the rate of mass change in the SETP is calculated to be -5.13 ± 2.55 Gt/yr.

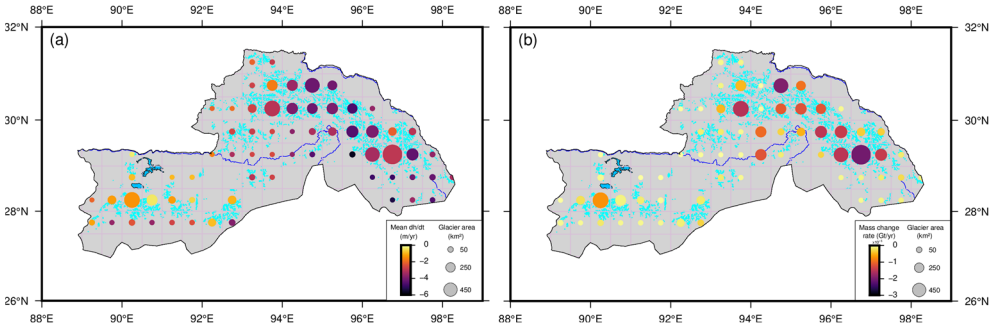

Figure 5. Spatial distribution of glacier changes in the SETP. (**a**) Glacier elevation change rate. (**b**) Glacier mass change rate.

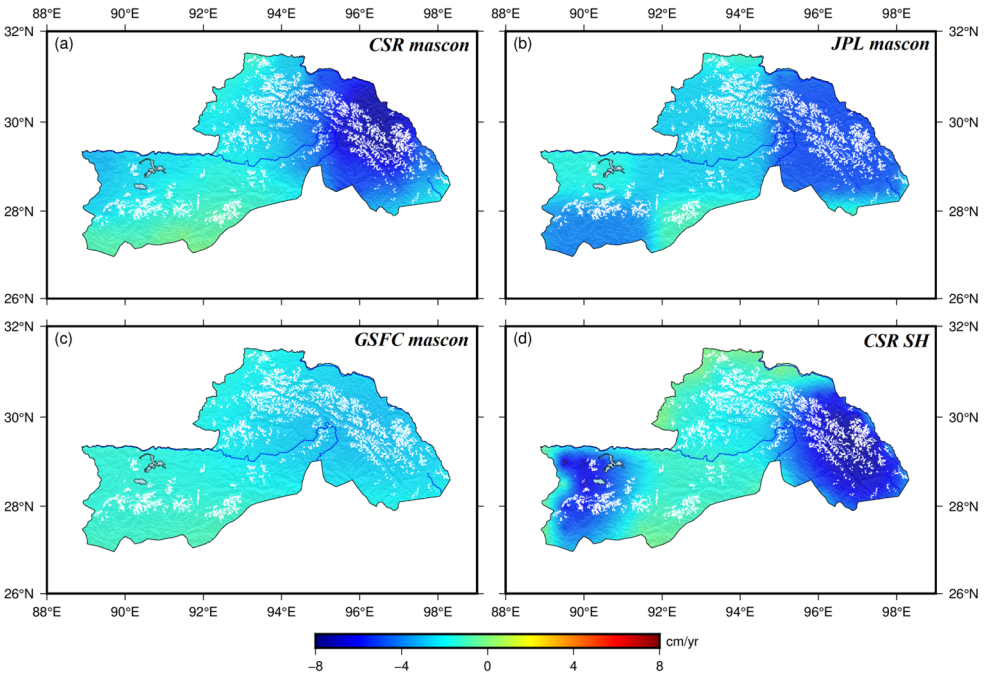

Figure 6. The mass change rates constrained by GRACE-FO mascon solutions in the SETP from 2018 to 2022. (**a**–**d**) show the long-term trends in TWS change in the form of equivalent water height (EWH) in the SETP inferred from CSR, JPL, GSFC mascon, and CSR SH products.

4.3. Variation in Land Water Storage Based on the Hydrological Model

The GRACE can observe changes in the gravity field caused by mass redistribution, including changes in surface and groundwater storage. In this research, a multi-source hydrological model was used to obtain changes in each hydrological component from October 2018 to October 2022 (Figure 7). Figure 7a illustrates the spatial distribution and trends in soil moisture in the SETP over the past four years, as inferred from the Noah and CPC mean values [5]. To highlight the differences between them, we used equivalent water height to express all hydrological components and used a uniform colorbar. The findings indicate spatial variability in soil moisture trends with an overall mass increase change of 1.88 ± 1.83 Gt/yr. To further investigate the specific variations in liquid water in the SETP, the WaterGAP Global Hydrology Model (WGHM) was applied to assess changes in groundwater (Figure 7b). The results reveal a consistent increase in groundwater. Given that the ICESat-2 is unable to precisely differentiate between glaciers and snow, we examined the snow changes outside the glacier-covered regions separately. As shown in Figure 7c, the snow mass change is relatively minor, at only −0.44 ± 0.09 Gt/yr. Although the lake shown in Figure 7d covers only a small part of the land surface, it provides unique information about how lake water changes. In the context of the overall rising trend for liquid water in the SETP, the lake water mass exhibited a decrease of −0.06 ± 0.02 Gt/yr since the change in lake water level is affected by factors such as precipitation, evaporation, and temperature. However, in recent years, the increasing temperature and the decreasing precipitation have led to decreasing water levels in the lake [57]. The variations in each hydrological component indicate that the soil moisture and groundwater mitigate the SETP mass loss to some extent, but there is little contribution from SWE or lakes to the TWS change.

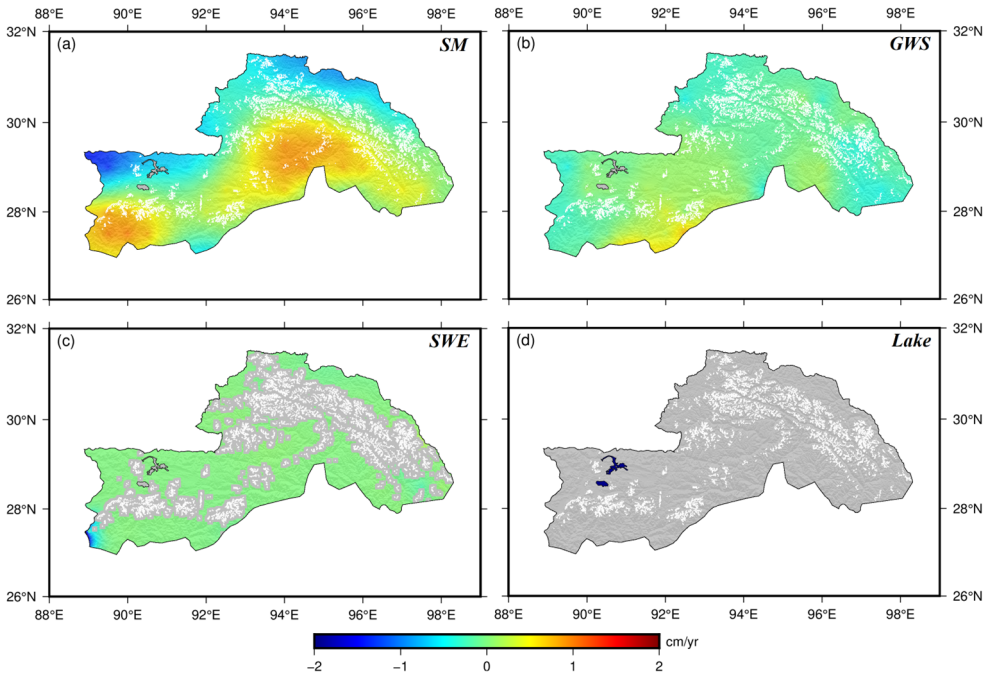

Figure 7. Variation trends in different hydrological components. (**a**) Soil moisture. (**b**) Groundwater output from WaterGAP. (**c**) Snow equivalent of GLDAS output. (**d**) Lake water trends.

5. Discussion

5.1. Comparison with Previous Studies

Many studies [2,17,20,34] have consistently indicated that glaciers in the SETP experience the most severe losses in the whole Tibetan Plateau (Figure 8). Notably, a series of satellite altimetry and remote sensing image analyses revealed varied rates of glacial decline. These include loss rates of −0.81 ± 0.32 m/yr (2003–2009) [58], −1.34 ± 0.29 m/yr (2003–2008) [36], −0.72 ± 0.27 m/yr (2000–2016) [20], −0.66 ± 0.24 m/yr (2000–2017) [29], −1.07 ± 0.10 m/yr

(2003–2019) [25], -1.11 ± 0.11 m/yr (2010–2019) [59], and -0.97 ± 0.59 m/yr (2018–2020) [2]. Our research estimates that the glacial loss in the SETP was -0.91 ± 0.18 m/yr over the period 2018–2022. This rate is notably higher than the -0.79 ± 0.09 m/yr estimated by Yi et al. [17] for the same region, suggesting an accelerated rate of glacial decline. The observed discrepancy could be primarily attributed to the ongoing global climate warming, which accelerates the melting rate of glaciers. Concurrently, a progressive decrease in summer precipitation contributes to this trend by increasing the net melting and reducing the accumulation of glaciers. This synergy results in an intensified and sustained glacier melt.

Previous research [17,25,34,41] has consistently demonstrated that the Nyainqentanglha Mountains in the SETP experience the most significant glacier mass loss. Statistically, the SETP glacier loss rate gradually slowed down from 2003 to 2019, from -1.07 ± 0.10 m/yr in the Nyainqentanglha Mountains to -0.59 ± 0.10 m/yr in the Himalayas [25]. The canyon topography of these regions serves as a significant conduit for the ingress of warm and moist air into the Tibetan Plateau. Both the Nyainqentanglha and Himalayas are geomorphological features of alpine valleys; thus, warm and moist air more easily reaches these regions [41]. Notably, the primary route for the Indian Ocean monsoon into the Tibetan Plateau is through the SETP, where the glaciers are predominantly maritime. As a result, the SETP has been identified as the region undergoing the most severe glacier loss across the entire Tibetan Plateau.

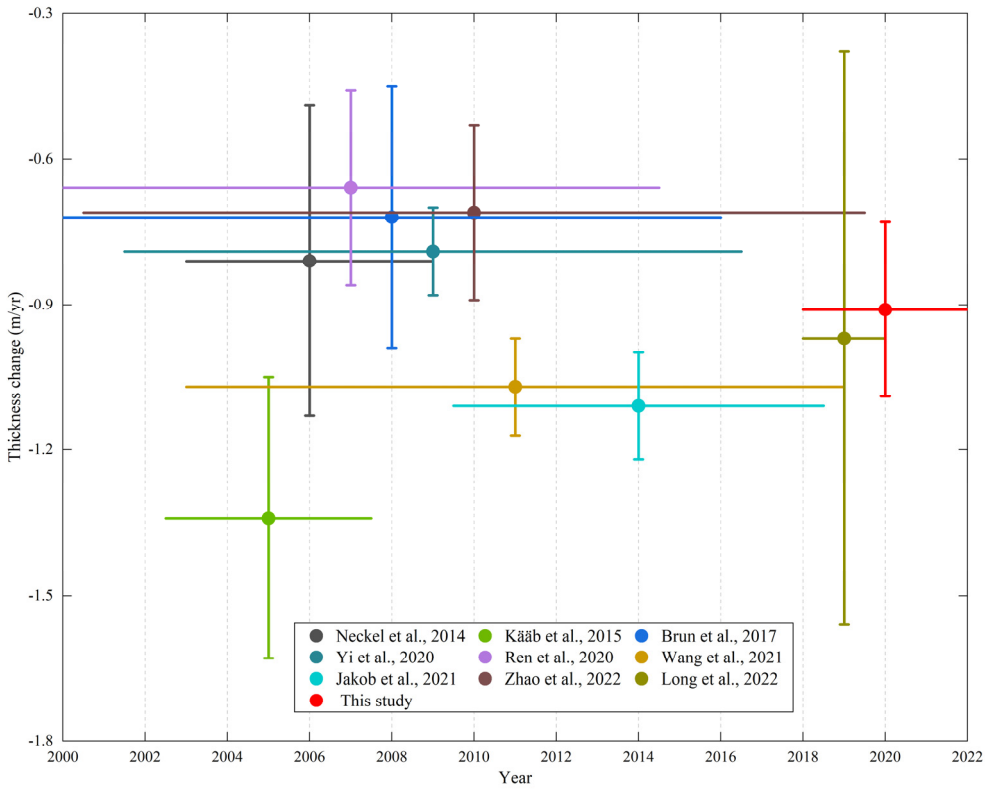

Figure 8. Comparison of our results and previous studies [2,16,20,25,29,36,41,58,59].

5.2. Contribution of Glacier Mass Loss to Land Water Mass Change in the SETP

This study offers a comprehensive evaluation of the mass balance and glacier mass change in the SETP by integrating multiple observation data sources including the following: terrestrial water storage (TWS), glaciers, soil moisture (SM), lakes, snow water equivalent (SWE), and groundwater storage (GWS). In this study, owing to the inconsistency in the spatial extent of each hydrologic distribution, the trend in mass change for each hydrological component was selected as a metric to assess its respective contribution to the overall mass balance. Observations using GRACE-FO data show that the TWS in

the SETP decreased at a rate of -5.13 ± 2.55 Gt/yr between October 2018 and October 2022. In this period, the loss of glacier mass, as monitored by the ICESat-2, was notably more pronounced, registering at -7.61 ± 1.52 Gt/yr. In contrast, the changes in lake and snow exhibited few variations in mass balance. Specifically, the lake mass change was -0.06 ± 0.02 Gt/yr, while the SWE mass change in the SETP was -0.44 ± 0.09 Gt/yr. However, it is critical to note that both soil moisture and groundwater in the SETP exhibited an increasing trend, with rates of 1.88 ± 1.83 Gt/yr and 1.45 ± 0.70 Gt/yr, respectively. When combining independent estimates of mass change in glaciers, lakes, snow, soil moisture, and groundwater, we found that the sum of mass changes in these components in the SETP was consistent with the overall mass change in TWS. This consistency underscores the multi-faceted nature of hydrological change and highlights the intricate interplay between various components in the SETP.

In this study, we adopted an innovative methodology to analyze mass changes in various hydrological components—glaciers, lakes, snow cover, soil moisture, and groundwater—using TWS changes as a baseline unit. This approach enabled us to quantitatively discern the relative contributions of each component to the mass balance in the SETP, as depicted in Figure 9a. Our findings reveal that glacier mass loss is the main cause of total mass loss in the SETP, accounting for 148% of the TWS mass change. Second, the mass loss in SWE and lake contributed to 9% and 2% of the TWS mass change, respectively. Moreover, Figure 9b presents a decrease in summer precipitation that is concurrent with an increase in liquid water components (soil moisture and groundwater) in the SETP (Figure 9a). This suggests that the substantial melting of solid water components—specifically, glaciers and snow—is a significant contributor to the increase in liquid water components. Intriguingly, the increase in liquid water exerts a counteracting effect on the overall mass balance: soil moisture and groundwater mitigate 37% and 28% of the TWS reduction, respectively. These findings not only underscore the critical role of dramatic glacier mass loss in the overall mass reduction in the SETP but also shed light on the intricate interplay of various components within the regional water cycle. Moreover, our analysis discerned a discrepancy in closure between the cumulative sum of alterations in various hydrological components and the TWS data ascertained via the GRACE-FO satellite. This inconsistency indicates potential errors inherent in hydrological models and observational methodologies and also suggests the presence of non-hydrological signals within the GRACE-FO observations, indicating the presence of active tectonic shifts within the SETP [60–62]. In addition, it may also be affected by permafrost melting, but the permafrost change over the Tibetan Plateau is mainly concentrated in the inland area, and its contribution to TWS change should be very small in our study area [63].

5.3. Dominant Factors of Glacier Seasonal Variation in the SETP

Marine glaciers exhibit a high sensitivity to climatic variations, thereby rendering climate a pivotal factor influencing glacial dynamics. The accumulation of glacial mass is primarily governed by precipitation, while temperature is the key determinant in glacial melting [47]. Notably, shifts in precipitation and temperature are critical driving forces in glacial transformations [2,64]. Studies have shown that the SETP temperature shows an upward trend, with an average warming rate of 0.23 °C/(10 yr) in the whole region, especially in the winter when the warming rate reaches 0.3 °C/(10 yr) [3,41]. Empirical data from various meteorological stations across different glacial territories corroborate this warming pattern [19,65]. Consequently, the escalating temperatures contribute to an extended glacial melting period, thereby exacerbating glacial ablation.

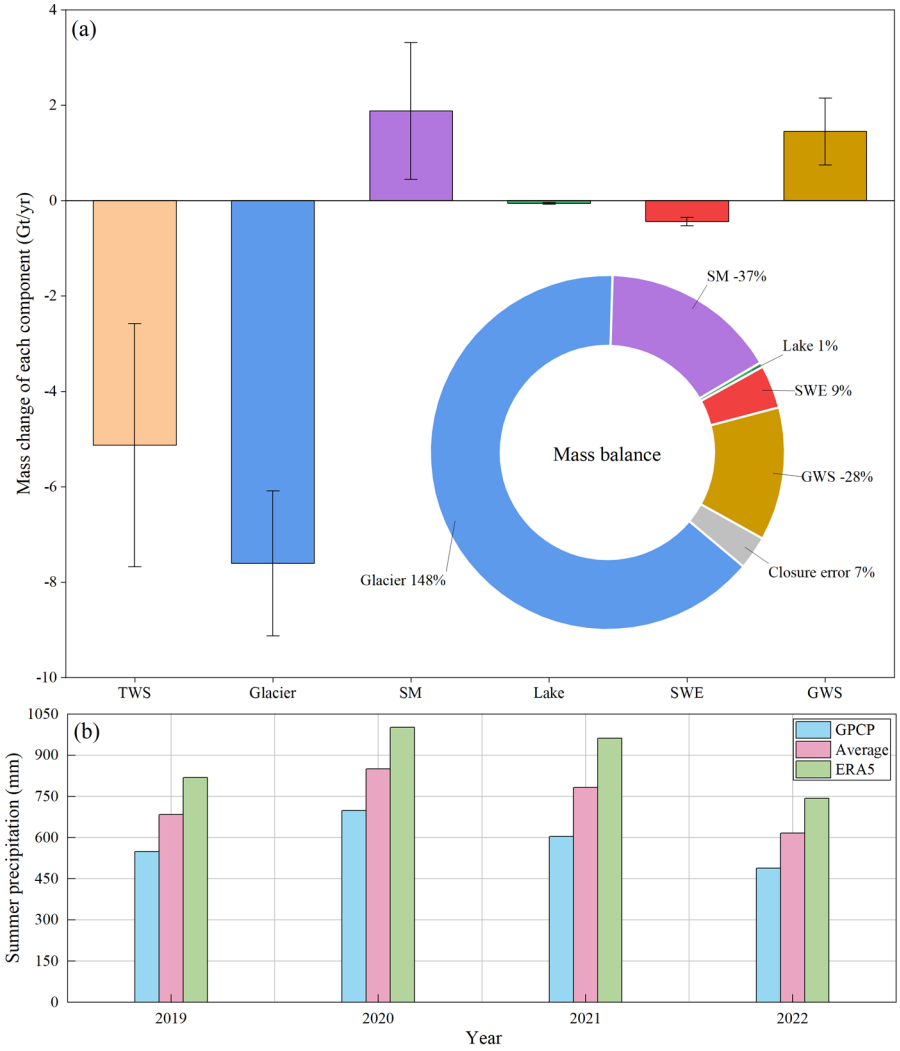

Figure 9. Mass balance and summer precipitation in the SETP for the period from 2018 to 2022. (**a**) Mass change of each land water component in the SETP. Inset shows the mass ratios of each land water component to total land water. (**b**) The variation of summer precipitation from October 2018 to October 2022.

This study delineated the interrelations among seasonal variations in glacier thickness, precipitation, and temperature, as depicted in Figure 10. We presented the seasonal changes in glaciers using average glacier thickness changes for each month between 2018 and 2022 (Figure 10a), and the same method was used to obtain the monthly average data for temperature and precipitation (Figure 10b). The peak temperature occurs in August and the minimum glacier thickness occurs in September, which is consistent with the finding of a previous study that indicated the peak temperature is one month earlier than the minimum glacier thickness [56]. This result indicates that the ice body temperature of the marine glacier is comparatively higher, which suggests an increased sensitivity to climatic changes. Figure 10a illustrates the accumulation pattern of SETP glaciers, which begins in the early winter and peaks during the spring season. Both precipitation models indicate a gradual increase in SETP precipitation throughout the spring. During this period, the temperature remains low, which facilitates the spring precipitation's role in augmenting glacier accumulation [17,66]. Precipitation in the SETP is mainly concentrated in the summer, with the peak occurring in July. While this abundant summer precipitation potentially contributes to regional glacier accumulation, concurrently rising temperatures limit this process. The lowest value of glacier thickness occurs in the autumn, mainly due to the effect of summer melting, low precipitation, and compaction. The compaction

effect should be accompanied by a glacial change in all seasons, especially in the summer when precipitation increases and rain infiltrates snow and ice, slowly transforming into ice under the compression of the covered snow [67]. Wang et al. [56] utilized two years of ICESat-2 data to observe changes in glacier thickness in the Indian Ocean monsoon region, including the SETP; the thickness exhibited a sawtooth pattern in September and October. However, our study used ICESat-2 data over a longer period to monitor the change in glacier thickness in the SETP, and the sawtooth shape phenomenon was also found. Annual variations in the precipitation show that the precipitation decreased month by month after the peak in July, and there was no precipitation sawtooth phenomenon. This indicates that glacier thickness experiences a rapid decrease following the high-temperature and heavy precipitation conditions of the summer but gradually begins to recover as precipitation and temperatures decline. Decreasing glaciers under high-temperature and heavy rain conditions should be related to the rain-on-snow events, which are known to increase melting at high elevations.

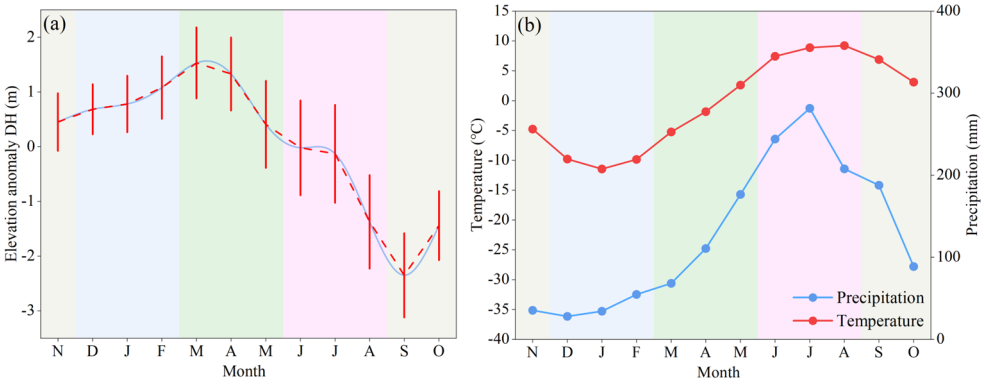

Figure 10. Comparison of seasonal changes in glacier thickness and seasonal changes in precipitation/temperature. (**a**) The seasonal cycle of glacier thickness based on the 4-year average in the period 2018–2022. (**b**) The seasonal cycle of precipitation/temperature based on the 4-year average in the period 2018–2022.

The unique combination of glacier typology and the specific monsoonal climate in the SETP results in significant glacier accumulation during both the winter and summer, especially in the summer [68]. In an effort to elucidate the influence of temperature and precipitation on glacier mass balance, we implemented an analytical exploration of their interrelationships, as illustrated in Figure 11. Previous studies have shown that temperature is the main factor affecting the mass balance of glaciers [69,70]. Yi et al. [17] compared annual mass loss (May–October) and summer temperature (June–August) to determine the impact of climate variables on glacier mass and found a correlation coefficient R = −0.59. This finding underscores the sensitivity of glacier mass balance to summer temperature fluctuations. We analyzed the seasonal cycle of glacier thickness, precipitation, and temperature from 2018 to 2022. Figure 11a presents a marked negative correlation between temperature and glacier thickness, with a correlation coefficient (R) of −0.70, suggesting that temperature changes predominantly govern the seasonal glacier cycle. Figure 11c shows the seasonal variation relationship between temperature and precipitation, and the correlation coefficient R = 0.91 indicates that the increase in temperature occurs with the simultaneous increase in precipitation, which hinders the accumulation of SETP glaciers in the summer. In addition, this study also unveiled a correlation coefficient between glacier thickness and precipitation change of −0.48 (Figure 11b), suggesting an inconclusive relationship and indicating that changes in glacier thickness cannot be solely attributed to precipitation. In summation, while temperature variations appear to be the primary driver of SETP glacier thickness variations, the interplay between temperature and precipitation also holds a significant role.

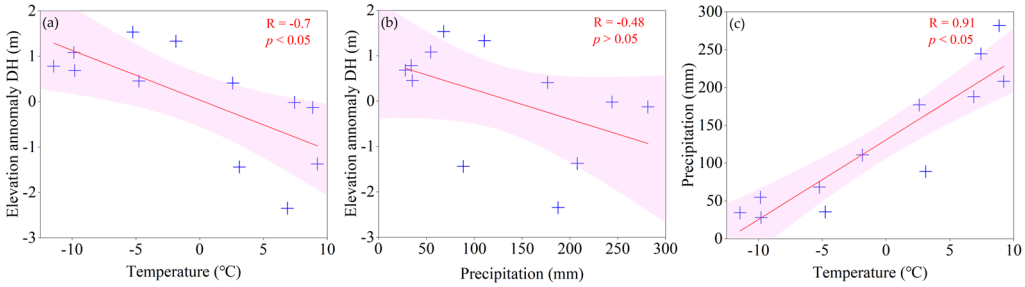

Figure 11. Correlation analysis of glacier thickness, temperature, and precipitation. (**a**) Correlation between glacier thickness and temperature. (**b**) Correlation between glacier thickness and precipitation. (**c**) Correlation between precipitation and temperature. The lines and shaded areas represent the linear function and 95% confidence intervals fitted to the data, respectively.

6. Conclusions

This study, based on ICESat-2 and GRACE-FO data and various hydrological models, focused on glacier mass loss and its consequent impact on land water storage change in the southeastern Tibetan Plateau (SETP) during a 49-month period from October 2018 to October 2022. Our findings can be summarized as follows:

(1) The glaciers in the SETP are melting rapidly, and the ICESat-inferred average thickness change rate is -0.91 ± 0.18 m/yr. It is important to note the difference in the spatial distribution of thickness change, with a more rapid decline in the eastern part of the SETP, where the maximum decrease rate reaches -5.71 m/yr. The diminishing thickness of glaciers has led to a significant mass loss of -7.61 ± 1.52 Gt/yr and shows signs of further acceleration.

(2) The GRACE-inferred terrestrial water storage (TWS) change in the SETP is experiencing a declining trend, with a rate of -5.13 ± 2.55 Gt/yr. Furthermore, the change rates of snow, lakes, soil moisture, and groundwater, as estimated through various hydrological models, are -0.44 ± 0.09 Gt/yr, -0.06 ± 0.02 Gt/yr, 1.88 ± 1.83 Gt/yr, and 1.45 ± 0.70 Gt/yr, respectively. Their corresponding proportional contributions to land water are 9%, 1%, −37%, and −28%, respectively. These findings underscore pronounced glacier mass loss as the primary driving factor of land water mass loss within the SETP.

(3) Compared with precipitation ($R = -0.48$, $p > 0.05$), temperature ($R = -0.7$, $p < 0.05$) has a stronger correlation with glacier thickness change. The SETP is characterized by a decreasing trend in solid water components (glacier and snow), while liquid water components (lakes, soil moisture, and groundwater) are either maintaining equilibrium or showing an increased trend. This highlights the compensatory effect of meltwater on land-based liquid water.

Author Contributions: Conceptualization, J.T. and J.J.; methodology, J.T.; software, J.T.; validation, J.T., B.Y. and J.J.; formal analysis, J.T.; investigation, J.T.; resources, Z.S.; data curation, B.Y.; writing—original draft preparation, J.T.; writing—review and editing, B.Y., J.J. and Z.T.; visualization, J.T.; supervision, J.J.; project administration, Z.S.; funding acquisition, Z.S., J.J. and Z.T. All authors have read and agreed to the published version of the manuscript.

Funding: This research was funded by the National Natural Science Foundation of China (Grant No. 42174054 of Zhen Shi, No. 42304020 of Jiashuang Jiao, No. 42104003 of Zhen Tian), the Natural Science Basic Research Program of Shaanxi (No. 2022JZ-17 of Zhen Shi), the Open Fund of Wuhan Gravitation and Solid Earth Tides National Observation and Research Station (WHYWZ202202 of Jiashuang Jiao), and Xianyang Key Research and Development Program of Chain (L2023-ZDYF-SF-006 of Zhen Tian), Sponsored by State Key Laboratory of Earthquake Dynamics (Project No. LED2022B02 of Zhen Tian).

Data Availability Statement: The CSR mascon data and CSR SH data supporting this study's findings are available in the Center for Space Research (http://www2.csr.utexas.edu/grace, accessed on 6 July 2023). The JPL mascon data supporting this study's findings are available in the Jet Propulsion

Laboratory (https://podaac.jpl.nasa.gov, accessed on 6 July 2023). The GSFC mascon data supporting this study's findings are available in the Goddard Space Flight Center (https://earth.gsfc.nasa.gov, accessed on 6 July 2023). Groundwater data can be accessed via http://www.watergap.de/ListOfPubl.html (accessed on 6 Aug 2023). Soil moisture data are available from the National Aeronautics and Space Administration (https://hydro1.gesdisc.eosdis.nasa.gov/data/GLDAS/, accessed on 5 July 2023) and the NOAA Physical Sciences Laboratory (https://psl.noaa.gov/data/gridded/data.cpcsoil.html, accessed on 18 Aug 2023).

Acknowledgments: The authors thank the editors and three anonymous reviewers for their significant suggestions and comments that helped improve this manuscript.

Conflicts of Interest: The authors declare no conflicts of interest.

References

1. Yao, T.; Thompson, L.; Yang, W.; Yu, W.; Gao, Y.; Guo, X.; Yang, X.; Duan, K.; Zhao, H.; Xu, B. Different glacier status with atmospheric circulations in Tibetan Plateau and surroundings. *Nat. Clim. Chang.* **2012**, *2*, 663–667. [CrossRef]
2. Di, L.; Xueying, L.; Xingdong, L.; Pengfei, H.; Fanyu, Z.; Zhongkun, H.; Yiming, W.; Fuqiang, T. Remote sensing retrieval of water storage changes and underlying climatic mechanisms over the Tibetan Plateau during 2000–2020. *Adv. Water Sci.* **2022**, *33*, 375–389. [CrossRef]
3. Yin, Z.; Yong, Z.; Shiyin, L.; Xin, W. Review of maritime glacier mass balance in the southeastern Tibetan Plateau. *J. Glaciol. Geocryol.* **2022**, *44*, 930–945.
4. Fujita, K.; Suzuki, R.; Nuimura, T.; Sakai, A. Performance of ASTER and SRTM DEMs, and their potential for assessing glacial lakes in the Lunana region, Bhutan Himalaya. *J. Glaciol.* **2008**, *54*, 220–228. [CrossRef]
5. Song, C.; Ke, L.; Huang, B.; Richards, K.S. Can mountain glacier melting explains the GRACE-observed mass loss in the southeast Tibetan Plateau: From a climate perspective? *Glob. Planet. Chang.* **2015**, *124*, 1–9. [CrossRef]
6. Ninglian, W.; Tandong, Y.; Baiqing, X.; An'an, C.; Weicai, W. Spatiotemporal Pattern, Trend, and Influence of Glacier Change in Tibetan Plateau and Surroundings under Global Warming. *Bull. Chin. Acad. Sci.* **2019**, *34*, 1220–1232. [CrossRef]
7. Qin, D.; Zhou, B.; Xiao, C. Progress in studies of cryospheric changes and their impacts on climate of China. *J. Meteorol. Res.* **2014**, *28*, 732–746. [CrossRef]
8. Bolch, T.; Kulkarni, A.; Kääb, A.; Huggel, C.; Paul, F.; Cogley, J.G.; Frey, H.; Kargel, J.S.; Fujita, K.; Scheel, M. The state and fate of Himalayan glaciers. *Science* **2012**, *336*, 310–314. [CrossRef] [PubMed]
9. Yao, T.; Xue, Y.; Chen, D.; Chen, F.; Thompson, L.; Cui, P.; Koike, T.; Lau, W.K.-M.; Lettenmaier, D.; Mosbrugger, V. Recent third pole's rapid warming accompanies cryospheric melt and water cycle intensification and interactions between monsoon and environment: Multidisciplinary approach with observations, modeling, and analysis. *Bull. Am. Meteorol. Soc.* **2019**, *100*, 423–444. [CrossRef]
10. Lee, H.; Calvin, K.; Dasgupta, D.; Krinner, G.; Mukherji, A.; Thorne, P.; Trisos, C.; Romero, J.; Aldunce, P.; Barrett, K. *Climate Change 2023: Synthesis Report. Contribution of Working Groups I, II and III to the Sixth Assessment Report of the Intergovernmental Panel on Climate Change*; The Australian National University: Canberra, Australia, 2023.
11. Immerzeel, W.W.; van Beek, L.P.H.; Bierkens, M.F.P. Climate Change Will Affect the Asian Water Towers. *Science* **2010**, *328*, 1382–1385. [CrossRef]
12. Pritchard, H.D. Asia's shrinking glaciers protect large populations from drought stress. *Nature* **2019**, *569*, 649–654. [CrossRef] [PubMed]
13. Yida, X.; Feiteng, W.; Shihai, H.; Canwen, Z. Test research on slowing down glacier melting by artificial intervention: A case study of Dagu Glacier. *J. Glaciol. Geocryol.* **2021**, *43*, 1878–1887.
14. Zun-lan, C.; Ping-yi, Z.; Chao, D.; Jing-jing, L. Hazards of Debris Flow due to Glacier-Lake Outburst in Southeastern Tibet. *J. Glaciol. Geocryol.* **2008**, *30*, 954–959.
15. Zhou, Y.; Li, Z.; Li, J.; Zhao, R.; Ding, X. Glacier mass balance in the Qinghai–Tibet Plateau and its surroundings from the mid-1970s to 2000 based on Hexagon KH-9 and SRTM DEMs. *Remote Sens. Environ.* **2018**, *210*, 96–112. [CrossRef]
16. Jansson, P.; Hock, R.; Schneider, T. The concept of glacier storage: A review. *J. Hydrol.* **2003**, *282*, 116–129. [CrossRef]
17. Yi, S.; Song, C.; Heki, K.; Kang, S.; Wang, Q.; Chang, L. Satellite-observed monthly glacier and snow mass changes in southeast Tibet: Implication for substantial meltwater contribution to the Brahmaputra. *Cryosphere* **2020**, *14*, 2267–2281. [CrossRef]
18. Shi, Y.; Liu, S. Estimation on the response of glaciers in China to the global warming in the 21st century. *Chin. Sci. Bull.* **2000**, *45*, 668–672. [CrossRef]
19. Yang, W.; Guo, X.; Yao, T.; Zhu, M.; Wang, Y. Recent accelerating mass loss of southeast Tibetan glaciers and the relationship with changes in macroscale atmospheric circulations. *Clim. Dyn.* **2016**, *47*, 805–815. [CrossRef]
20. Brun, F.; Berthier, E.; Wagnon, P.; Kääb, A.; Treichler, D. A spatially resolved estimate of High Mountain Asia glacier mass balances from 2000 to 2016. *Nat. Geosci.* **2017**, *10*, 668–673. [CrossRef] [PubMed]
21. Maurer, J.M.; Schaefer, J.; Rupper, S.; Corley, A. Acceleration of ice loss across the Himalayas over the past 40 years. *Sci. Adv.* **2019**, *5*, eaav7266. [CrossRef] [PubMed]
22. Gao, J.; Du, J.; Yixi, Z. Forewarning Model for Glacial Lake Outburst in Southeast Tibet. *Appl. Sci.* **2023**, *13*, 1797. [CrossRef]

23. Rounce, D.R.; Hock, R.; Shean, D.E. Glacier Mass Change in High Mountain Asia Through 2100 Using the Open-Source Python Glacier Evolution Model (PyGEM). *Front. Earth Sci.* **2020**, *7*, 331. [CrossRef]
24. Yang, W.; Yao, T.; Xu, B.; Wu, G.; Ma, L.; Xin, X. Quick ice mass loss and abrupt retreat of the maritime glaciers in the Kangri Karpo Mountains, southeast Tibetan Plateau. *Chin. Sci. Bull.* **2008**, *53*, 2547–2551. [CrossRef]
25. Wang, Q.; Yi, S.; Sun, W. Continuous estimates of glacier mass balance in high mountain Asia based on ICESat-1, 2 and GRACE/GRACE follow-on data. *Geophys. Res. Lett.* **2021**, *48*, e2020GL090954. [CrossRef]
26. Liu, L.; Jiang, L.; Jiang, H.; Wang, H.; Ma, N.; Xu, H. Accelerated glacier mass loss (2011–2016) over the Puruogangri ice field in the inner Tibetan Plateau revealed by bistatic InSAR measurements. *Remote Sens. Environ.* **2019**, *231*, 111241. [CrossRef]
27. Wu, K.; Liu, S.; Jiang, Z.; Xu, J.; Wei, J.; Guo, W. Recent glacier mass balance and area changes in the Kangri Karpo Mountains from DEMs and glacier inventories. *Cryosphere* **2018**, *12*, 103–121. [CrossRef]
28. Cao, B.; Pan, B.; Wen, Z.; Guan, W.; Li, K. Changes in glacier mass in the Lenglongling Mountains from 1972 to 2016 based on remote sensing data and modeling. *J. Hydrol.* **2019**, *578*, 124010. [CrossRef]
29. Ren, S.; Menenti, M.; Jia, L.; Zhang, J.; Zhang, J.; Li, X. Glacier mass balance in the Nyainqentanglha Mountains between 2000 and 2017 retrieved from ZiYuan-3 stereo images and the SRTM DEM. *Remote Sens.* **2020**, *12*, 864. [CrossRef]
30. Long, D.; Shen, Y.; Sun, A.; Hong, Y.; Longuevergne, L.; Yang, Y.; Li, B.; Chen, L. Drought and flood monitoring for a large karst plateau in Southwest China using extended GRACE data. *Remote Sens. Environ.* **2014**, *155*, 145–160. [CrossRef]
31. Sun, Z.; Long, D.; Yang, W.; Li, X.; Pan, Y. Reconstruction of GRACE data on changes in total water storage over the global land surface and 60 basins. *Water Resour. Res.* **2020**, *56*, e2019WR026250. [CrossRef]
32. Jiao, J. Mass Transports in the Tibetan Plateau and Fennoscandia Revealed by Satellite Gravimetry. Ph.D. Thesis, Chang'an University, Xi'an, China, 2020.
33. He, M.; Li, Z.; Jiang, W.; Pan, Y.; Jiao, J.; Xiao, Y. Seasonal and Interannual Fluctuations of Glacier Mass balance and Climate Response Processes on the Tibetan Plateau Based on GRACE/GRACE-FO. *IEEE Trans. Geosci. Remote Sens.* **2023**, *61*, 4301709. [CrossRef]
34. Kääb, A.; Berthier, E.; Nuth, C.; Gardelle, J.; Arnaud, Y. Contrasting patterns of early twenty-first-century glacier mass change in the Himalayas. *Nature* **2012**, *488*, 495–498. [CrossRef] [PubMed]
35. Gardelle, J.; Berthier, E.; Arnaud, Y.; Kääb, A. Region-wide glacier mass balances over the Pamir-Karakoram-Himalaya during 1999–2011. *Cryosphere* **2013**, *7*, 1263–1286. [CrossRef]
36. Kääb, A.; Treichler, D.; Nuth, C.; Berthier, E. Brief Communication: Contending estimates of 2003–2008 glacier mass balance over the Pamir–Karakoram–Himalaya. *Cryosphere* **2015**, *9*, 557–564. [CrossRef]
37. Treichler, D.; Kääb, A. ICESat laser altimetry over small mountain glaciers. *Cryosphere* **2016**, *10*, 2129–2146. [CrossRef]
38. Smith, B.; Fricker, H.A.; Gardner, A.S.; Medley, B.; Nilsson, J.; Paolo, F.S.; Holschuh, N.; Adusumilli, S.; Brunt, K.; Csatho, B. Pervasive ice sheet mass loss reflects competing ocean and atmosphere processes. *Science* **2020**, *368*, 1239–1242. [CrossRef] [PubMed]
39. Yao, T.; Pu, J.; Lu, A.; Wang, Y.; Yu, W. Recent glacial retreat and its impact on hydrological processes on the Tibetan Plateau, China, and surrounding regions. *Arct. Antarct. Alp. Res.* **2007**, *39*, 642–650. [CrossRef]
40. Consortium, R. *Randolph Glacier Inventory—A Dataset of Global Glacier Outlines, Version 6 [Dataset]*; National Snow and Ice Data Center: Boulder, CO, USA, 2017.
41. Zhao, F.; Long, D.; Li, X.; Huang, Q.; Han, P. Rapid glacier mass loss in the Southeastern Tibetan Plateau since the year 2000 from satellite observations. *Remote Sens. Environ.* **2022**, *270*, 112853. [CrossRef]
42. Xu, Z.; Gong, T.; Li, J. Decadal trend of climate in the Tibetan Plateau—Regional temperature and precipitation. *Hydrol. Process. Int. J.* **2008**, *22*, 3056–3065. [CrossRef]
43. Li, C.; Jiang, L.; Liu, L.; Wang, H. Regional and altitude-dependent estimate of the SRTM C/X-band radar penetration difference on High Mountain Asia glaciers. *IEEE J. Sel. Top. Appl. Earth Obs. Remote Sens.* **2021**, *14*, 4244–4253. [CrossRef]
44. Scanlon, B.R.; Zhang, Z.; Save, H.; Wiese, D.N.; Landerer, F.W.; Long, D.; Longuevergne, L.; Chen, J. Global evaluation of new GRACE mascon products for hydrologic applications. *Water Resour. Res.* **2016**, *52*, 9412–9429. [CrossRef]
45. Chen, J.; Wilson, C.; Tapley, B.; Save, H.; Cretaux, J.F. Long-term and seasonal Caspian Sea level change from satellite gravity and altimeter measurements. *J. Geophys. Res. Solid Earth* **2017**, *122*, 2274–2290. [CrossRef]
46. Chen, J.; Wilson, C.; Li, J.; Zhang, Z. Reducing leakage error in GRACE-observed long-term ice mass change: A case study in West Antarctica. *J. Geod.* **2015**, *89*, 925–940. [CrossRef]
47. Jiao, J.; Zhang, Y.; Bilker-Koivula, M.; Poutanen, M.; Yin, P.; Zhang, Y. Interannual glacier and lake mass changes over Scandinavia from GRACE. *Geophys. J. Int.* **2020**, *221*, 2126–2141. [CrossRef]
48. Bi, H.; Ma, J.; Zheng, W.; Zeng, J. Comparison of soil moisture in GLDAS model simulations and in situ observations over the Tibetan Plateau. *J. Geophys. Res. Atmos.* **2016**, *121*, 2658–2678. [CrossRef]
49. Huang, J.; van den Dool, H.M.; Georgarakos, K.P. Analysis of model-calculated soil moisture over the United States (1931–1993) and applications to long-range temperature forecasts. *J. Clim.* **1996**, *9*, 1350–1362. [CrossRef]
50. Chen, M.; Xie, P.; Janowiak, J.E.; Arkin, P.A. Global land precipitation: A 50-yr monthly analysis based on gauge observations. *J. Hydrometeorol.* **2002**, *3*, 249–266. [CrossRef]
51. Fan, Y.; Van den Dool, H. A global monthly land surface air temperature analysis for 1948–present. *J. Geophys. Res. Atmos.* **2008**, *113*, D01103. [CrossRef]

52. Döll, P.; Müller Schmied, H.; Schuh, C.; Portmann, F.T.; Eicker, A. Global-scale assessment of groundwater depletion and related groundwater abstractions: Combining hydrological modeling with information from well observations and GRACE satellites. *Water Resour. Res.* **2014**, *50*, 5698–5720. [CrossRef]
53. Herbert, C.; Döll, P. Global assessment of current and future groundwater stress with a focus on transboundary aquifers. *Water Resour. Res.* **2019**, *55*, 4760–4784. [CrossRef]
54. Adler, R.F.; Huffman, G.J.; Chang, A.; Ferraro, R.; Xie, P.-P.; Janowiak, J.; Rudolf, B.; Schneider, U.; Curtis, S.; Bolvin, D. The version-2 global precipitation climatology project (GPCP) monthly precipitation analysis (1979–present). *J. Hydrometeorol.* **2003**, *4*, 1147–1167. [CrossRef]
55. Sun, F.; He, B.; Liu, C.; Zeng, Y. Comparison of Hydrological Patterns between Glacier-Fed and Non-Glacier-Fed Lakes on the Southeastern Tibetan Plateau. *Remote Sens.* **2021**, *13*, 4024. [CrossRef]
56. Wang, Q.; Sun, W. Seasonal Cycles of High Mountain Asia Glacier Surface Elevation Detected by ICESat-2. *J. Geophys. Res. Atmos.* **2022**, *127*, e2022JD037501. [CrossRef]
57. Handuo, T.; Yangzong, C.; Chen, Z.; Fan, Z. Characteristics of the lake water level changes and influencing factors in Yamzhog Yumco in Tibet from 1974 to 2019. *J. Arid. Land Resour. Environ.* **2021**, *35*, 83–89. [CrossRef]
58. Neckel, N.; Kropáček, J.; Bolch, T.; Hochschild, V. Glacier mass changes on the Tibetan Plateau 2003–2009 derived from ICESat laser altimetry measurements. *Environ. Res. Lett.* **2014**, *9*, 014009. [CrossRef]
59. Jakob, L.; Gourmelen, N.; Ewart, M.; Plummer, S. Spatially and temporally resolved ice loss in High Mountain Asia and the Gulf of Alaska observed by CryoSat-2 swath altimetry between 2010 and 2019. *Cryosphere* **2021**, *15*, 1845–1862. [CrossRef]
60. Zhen, T.; Zhi-qiang, Y.; Shi-di, W. Moment Deficits on the Major Faults And Earthquake Hazard Assessment in the Eastern Himalayan Syntaxis. *Seismol. Geol.* **2020**, *42*, 33–49.
61. Tian, Z.; Freymueller, J.T.; Yang, Z. Spatio-temporal variations of afterslip and viscoelastic relaxation following the Mw 7.8 Gorkha (Nepal) earthquake. *Earth Planet. Sci. Lett.* **2020**, *532*, 116031. [CrossRef]
62. Jiao, J.; Zhang, Y.; Yin, P.; Zhang, K.; Wang, Y.; Bilker-Koivula, M. Changing Moho Beneath the Tibetan plateau revealed by GRACE observations. *J. Geophys. Res. Solid Earth* **2019**, *124*, 5907–5923. [CrossRef]
63. Xiang, L.; Wang, H.; Steffen, H.; Wu, P.; Jia, L.; Jiang, L.; Shen, Q. Groundwater storage changes in the Tibetan Plateau and adjacent areas revealed from GRACE satellite gravity data. *Earth Planet. Sci. Lett.* **2016**, *449*, 228–239. [CrossRef]
64. Feng, S.Y.; Song, Z.X. Climate change impacts on surface water resources in northwest arid area and the future trend. *Sci. Sin. (Chim.)* **1995**, *25*, 968–977. (In Chinese)
65. Kunpeng, W.; Shiyin, L.; Wanqin, G. Glacier variation and its response to climate change in the Mount Namjagbarwa from 1980 to 2015. *J. Glaciol. Geocryol.* **2020**, *42*, 1115–1125.
66. Yang, W.; Yao, T.; Guo, X.; Zhu, M.; Li, S.; Kattel, D.B. Mass balance of a maritime glacier on the southeast Tibetan Plateau and its climatic sensitivity. *J. Geophys. Res. Atmos.* **2013**, *118*, 9579–9594. [CrossRef]
67. Sturm, M.; Holmgren, J. Differences in compaction behavior of three climate classes of snow. *Ann. Glaciol.* **1998**, *26*, 125–130. [CrossRef]
68. Jouberton, A.; Shaw, T.E.; Miles, E.; McCarthy, M.; Fugger, S.; Ren, S.; Dehecq, A.; Yang, W.; Pellicciotti, F. Warming-induced monsoon precipitation phase change intensifies glacier mass loss in the southeastern Tibetan Plateau. *Proc. Natl. Acad. Sci. USA* **2022**, *119*, e2109796119. [CrossRef]
69. Cogley, J.G.; Arendt, A.; Bauder, A.; Braithwaite, R.; Hock, R.; Jansson, P.; Kaser, G.; Moller, M.; Nicholson, L.; Rasmussen, L. *Glossary of Glacier Mass Balance and Related Terms*; International Hydrological Programme: Paris, Fance, 2010.
70. Yang, W.; Zhao, C.; Westoby, M.; Yao, T.; Wang, Y.; Pellicciotti, F.; Zhou, J.; He, Z.; Miles, E. Seasonal dynamics of a temperate Tibetan glacier revealed by high-resolution UAV photogrammetry and in situ measurements. *Remote Sens.* **2020**, *12*, 2389. [CrossRef]